FULL LENGTH PAPER

HEAT FLUX PREDICTION IN A KEROSENE FUELLED SCRAMJET COMBUSTOR THROUGH CFD

Malsur Dharavath, P. Manna, Debasis Chakraborty
Directorate of Computational Dynamics
Defence Research and Development Laboratory (DRDL)
Kanchanbagh Post, Hyderabad-500 058
Email : debasis_cfd@drdl.drdo.in; debasis_drdl@yahoo.co.in

Abstract

Thermo-structural design of high speed propulsive systems require heat transfer as an input. Nonreacting and reacting flow simulations are carried out to predict the heat transfer characteristics of scramjet combustor using commercial software. The software employs finite volume method to solve 3-D RANS equations along with SST-kω turbulence model and infinitely fast chemistry. The flow through a convergent-divergent nozzle is taken as validation test case and very good match is obtained between computed heat flux and experimental data. It is observed that minimum 10 micron 1st grid spacing is required to predict wall heat flux accurately and grid independence of heat flux data is demonstrated. Heat transfer coefficient is independent of various isothermal walls and computed heat fluxes are higher at combustion intense zone behind fuel injection struts.

Keywords*: Reacting Flow, Scramjet Combustor, Grid Independence, Heat Flux*

Nomenclature

A_{ebu}, B_{ebu} = Model coefficient of EDM
C = Log-layer constant
D = Diameter
EDM = Eddy dissipation model
h = Height of the combustor entry, heat transfer coefficient
H = Enthalpy
i, j, k = Three axes direction
I = Species component
k = Turbulent kinetic energy
m = Mass flow
M = Molecular weight, Mach number
P = Pressure
Pr = Prandtl number
q = Heat flux
RANS = Reynolds Averaged Navier Stokes
S = Source term
SMD = Sauter mean diameter
SST = Shear Stress Transport
t = Time
T = Temperature
U = Velocity
X, Y, Z = Three axes direction
Y = Species mass fraction

Symbol

ΔF = Net thrust
Δn = Distance between wall to first grid point
v = Dispersion factor, stoichiometric coefficient, kinematic viscosity
ρ = Density
ϕ = Equivalence ratio
μ = Viscosity
τ = Shear stress
ω = Turbulent frequency
η = Efficiency
σ = Constant value of k, ε and ω terms
Ω = Strain rate

Subscript

air = Inflow air
aw = Adiabatic wall
C = Convective, combustion

Paper Code : V70 N2/1001-2018. Manuscript received on 25 Oct 2017. Reviewed, revised and accepted as a Full Length Contributed Paper on 16 Feb 2018

CI = Combustor entry
e = Exit
f, ox, p = Fuel or bulk fluid, oxidizer, product
I = Various species
k = x, y, z directions
l = Laminar
0 = Stagnation region
t = Turbulent, total
th = Thrust
w = Wall

Introduction

Starting from pioneering work of Ferri [1] in early 1960s, significant progress has been made in scramjet engine development of hypersonic air-breathing cruise vehicles for both civil and military applications. Both hydrogen and hydrocarbon fuels were studied extensively [2,3] for scramjet engines. Lower hypersonic ($M_\infty < 8$) flight regimes and volume limited applications necessitate hydrocarbon fuels [4] due to their greater density and ease of handling. Computational Fluid Dynamics (CFD) tools are employed to model accurately several complex physical processes during the design phase of the scramjet engine. To circumvent slow transport and reduced mixing of liquid fuel with incoming air stream, strut based injection system are preferred for flight sized hydrocarbon fuelled scramjet combustor. Computational studies of strut based scramjet combustor with liquid hydrocarbon are not reported adequately in open literature. Bouchez and co-authors [5,6] have used ONERA's in-house CFD code MSD-2.2.2 for simulation of strut-based kerosene fuelled scramjet combustor and reported reasonable match between computed wall static pressures and experimental data. Adequate details are not provided for two-phase reactive calculations. Manna et al. [7] studied the effect of the combustor inlet Mach number and total pressure on the combustion process in a strut-based kerosene fuelled scramjet combustor and concluded that predominant supersonic flow without thermal choking could be obtained through higher combustor entry Mach number and distributed fuel injection. The fuel injection struts caused significant flow blockage, made the flow fully three-dimensional and affected the mixing and combustion pattern in the scramjet combustor. Manna et al. [8] and Malsur et al. [9] have estimated the thrust and combustion efficiency parameters of a flight sized scramjet combustor. Combustor performance was improved significantly by redistributing the fuel injection holes, relocating the strut and prescribing proper drop size distribution. Malsur et al. [10] carried out end-to-end CFD simulation for a complete hypersonic vehicle integrating both external (nonreacting) and internal (reacting) flow together to calculate the scramjet combustor performance and vehicle net thrust and drag. The computational analysis provides net forces and moments of the whole vehicle to carry out the mission analysis.

Although CFD methods are being employed to predict the overall performance of the scramjet engine in terms of thrust and combustion efficiency, the use of these methods in thermo-structural design of combustor walls are rather limited. Malsur et al. [11] predicted convective heat flux in a hydrocarbon fuelled scramjet combustor. High temperature inside the combustor due to reaction of fuel with incoming air stream and external aerodynamic heating by ambient hypersonic flow are the major source of heat load for combustor walls. Wall heat flux and resulting surface temperature are the key inputs for thermo-structural design of scramjet combustor. Measurements of these parameters are very difficult due to severe thermal and oxidising environment of hypersonic flight Mach number. For example, at $M_\infty > 6$, the combustion product total temperature and average wall heat flux would be around 2800 K and 5.0 MW/m^2 [12]. Wall heat flux and temperature in a supersonic model combustor is measured by Li et al. [13] with an integrated water cooled sensor. Kennedy and Donbar [14] measured heat fluxes at four locations in a direct-connect gaseous hydrocarbon-fuelled cavity based scramjet combustor operating at fuel equivalence ratios of 0.6 to 1.0. Measured heat fluxes are higher (0.6 - 2.0 MW/m^2) at reaction zone of the cavity flame holder; whereas, upstream and downstream regions of the flame holder experience comparatively lower heat fluxes. Zhang et al. [15] used a state observer based method to estimate inner wall temperature from measured pressure and outer wall surface temperature of a scramjet combustor.

Well resolved CFD tools can easily locate hot spot (region of extreme heat load) of the scramjet combustor wall which may be difficult to estimate through theoretical or experimental studies. In the present work, commercial CFD software CFX [16] is first validated against experimentally measured heat flux data in supersonic convergent-divergent nozzle [17] and the convective heat flux (q_w) and heat transfer coefficient (h_c) are estimated of a flight sized kerosene fuelled scramjet combustor.

Computational Methodology

Three-dimensional Reynolds Averaged Navier Stokes (RANS) equations are solved along with species and turbulence transport equations using commercial CFD code

CFX [16]. The code is fully implicit finite volume method with finite element based discretization of geometry. The convective terms are discretized by 2nd order spatial scheme to capture the flow features more accurately. Menter's shear stress transport, *SST- k*ω [18] turbulence model is used along with wall functions in the present simulation.

Governing Equations

The system of governing equations describing the conservation of mass, momentum, energy and species transport equations of compressible gas flows are written as:

Conservation of Mass equation:

$$\frac{\partial \rho}{\partial t} + \frac{\partial}{\partial x_k}(\rho\, u_k) = 0 \qquad k = 1, 2, 3 \tag{1}$$

Conservation of Momentum equation:

$$\frac{\partial}{\partial t}(\rho\, u_i) + \frac{\partial}{\partial x_k}(\rho\, u_i\, u_k) + \frac{\partial P}{\partial x_i} = \frac{\partial (\tau_{ik})}{\partial x_k}, \qquad i, k = 1, 2, 3 \tag{2}$$

Conservation of Energy equation:

$$\frac{\partial}{\partial t}(\rho H) + \frac{\partial}{\partial x_k}(\rho\, u_k H) = -\frac{\partial}{\partial x_k}(u_j \tau_{jk}) + \frac{\partial q_k}{\partial x_k}, \quad j, k = 1,2,3 \tag{3}$$

Turbulence Transport Equations

k-ε Turbulence Model

Turbulent kinetic energy (k) equation:

$$\frac{\partial}{\partial t}(\rho\, k) + \frac{\partial}{\partial x_k}(\rho\, u_k\, k) = \frac{\partial}{\partial x_k}\left(\left(\frac{\mu_l}{Pr} + \frac{\mu_t}{\sigma_k}\right)\frac{\partial k}{\partial x_k}\right) + S_k \tag{4}$$

Turbulent eddy dissipation(ε)*equation*:

$$\frac{\partial}{\partial t}(\rho\, \varepsilon) + \frac{\partial}{\partial x_k}(\rho\, u_k\, \varepsilon) = \frac{\partial}{\partial x_k}\left(\left(\frac{\mu_l}{Pr} + \frac{\mu_t}{\sigma_\varepsilon}\right)\frac{\partial \varepsilon}{\partial x_k}\right) + S_\varepsilon \tag{5}$$

where, ρ, u_i, p, H are the density, velocity components, pressure and total energy respectively and $\mu = \mu_l + \mu_t$ is the total viscosity; μ_l, μ_t being the laminar and turbulent viscosity and Pr is the Prandtl number. The source terms S_k and S_ε of the k and ε equation are defined as

$$S_K = \tau_{ik}\frac{\partial u_i}{\partial x_k} - \rho\,\varepsilon \text{ and } S_\varepsilon = C_{\varepsilon 1}\tau_{ik}\frac{\partial u_i}{\partial x_k} - C_{\varepsilon 2}\,\frac{\rho \varepsilon^2}{k}$$

where turbulent shear stress is defined as

$$\tau_{ik} = \mu_t\left(\frac{\partial u_i}{\partial x_k} + \frac{\partial u_k}{\partial x_i}\right) \tag{6}$$

Laminar viscosity (μ_l) is calculated from Sutherland law as

$$\mu_l = \mu_{ref}\left(\frac{T}{T_{ref}}\right)^{3/2}\left(\frac{T_{ref} + S}{T + S}\right) \tag{7}$$

where, T is the temperature and μ_{ref}, T_{ref}, and S are known coefficient. The turbulent viscosity μ_t is calculated as

$$\mu_t = C_\mu \frac{\rho\, k^2}{\varepsilon} \tag{8}$$

The coefficients involved in the calculation of turbulent viscoeity (μ_t) are taken as

$c_\mu = 0.09$, $C_{\varepsilon 1} = 1.44$, $C_{\varepsilon 2} = 1.92$,

$\sigma_K = 1.0$, $\sigma_\varepsilon = 1.3$, $\sigma_c = 0.9$

The heat flux q_k is calculated as $q_k = -\lambda \frac{\partial T}{\partial x_k}$, λ is the coefficient of thermal conductivity

k-ω Turbulence Model

In this model, turbulent viscoeity is claculated as function of k and ω.

$$\mu_t = f\left(\frac{\rho k}{\omega}\right) \tag{9}$$

Turbulent kinetic energy (k) equation:

$$\frac{\partial}{\partial t}(\rho k) + \frac{\partial}{\partial x_i}(\rho\, k\, u_i) = \frac{\partial}{\partial x_j}\left(\Gamma_k \frac{\partial k}{\partial x_j}\right) + G_k - Y_k \tag{10}$$

*Specific dissipation rate (*ω*) equation*:

$$\frac{\partial}{\partial t}(\rho\omega)+\frac{\partial}{\partial x_i}(\rho\,\omega\,u_i)=\frac{\partial}{\partial x_j}\left(\Gamma_\omega\,\frac{\partial\omega}{\partial x_j}\right)+G_\omega-Y_\omega \qquad (11)$$

Where, G_k is turbulence production due to viscous and buoyance forces, $Y_k=\beta^1\,\rho\,k\,w$, $\Gamma_k=\mu+\frac{\mu_t}{\sigma_k}$,$G_w=\alpha\frac{\omega}{k}G_k$, $Y_w=\beta\,\rho\,w^2$ and $\Gamma_w=\mu+\frac{\mu_t}{\sigma_w}$ of the k and ω equations respectively. Where $\beta^1=0.09$, $\alpha=5/9$, $\beta=0.075$, and $\sigma_k=\sigma_w=2$

SST - $k\omega$ Turbulence Model

To retain the robust and accurate formulation of Wilcox's k- ω model in the near wall region, and take advantage of the free stream independence of the k- ε model in the outer part of the boundary layer, Menter [18] blended both the models through a switching function. k- ε model was transformed into Wilcox's k- ω formulation and was multiplied by (1-F_1) and added to original k- ω model multiplied by F_1. The blending function F_1 will be one in the near wall region and zero away from the surface. In the second step, the definition of eddy viscosity (μ_t) was modified in the following way to account for the transport of the principal turbulent shear stress ($\tau=-\rho\,\overline{u'v'}$)

$$v_t=\frac{a_1\,k}{\max(a_1\,\omega\,;\,\Omega\,F_2)} \qquad (12)$$

where v_t (is kinematic viscosity) = μ_t / ρ and F_2 is a blending function similar to F_1, which restricts the limiter to the wall boundary layer. Ω is an invariant measure of the strain rate. Their formulation is based on the distance to the nearest surface and on the flow variables.

$$F_2=\tanh(arg_2^4) \qquad (13)$$

The argument is defined as

$$arg_2=\min\left[\max\left\{\frac{\sqrt{k}}{0.09\,\omega\,y'},\frac{500\,v}{y^2\,\omega}\right\},\frac{4\,\rho\,\sigma_{\omega 2}\,k}{y^2\,CD_{k\omega}}\right] \qquad (14)$$

Where y is the distance to the wall and $CD_{k\omega}$ the positive portion of the cross-diffusion terms expressed as

$$CD_{k\omega}=\max\left[2\,\rho\,\sigma_{\omega 2}\,\frac{1}{\omega}\,\frac{\partial k}{\partial x_j}\,\frac{\partial\omega}{\partial x_j},\;10^{-20}\right] \qquad (15)$$

Where, y is the distance to the nearest wall and v is the kinematic viscosity

Species Transport Equation

Conservation of Species Mass Fraction (Y_I):

$$\frac{\partial}{\partial t}(\rho\,Y_I)+\frac{\partial}{\partial x_k}(\rho\,u_k\,Y_I)=\frac{\partial}{\partial x_k}\left[\left(\frac{\mu_l}{\mathrm{Pr}}+\frac{\mu_t}{\sigma_c}\right)\frac{\partial Y_I}{\partial x_k}\right]+S_I \qquad (16)$$

Where the source term S_I is due to the chemical reaction rate involving species component I, and Y_I is the mass fraction of I^{th} species. The chemical reactions can be described in terms of k elementary reactions involving N_C components that can be written as:

$$\sum_{I=A,\,B,\,C,\,\ldots}^{N_c} v_{kI}^{i}\,I \quad\leftrightarrow\quad \sum_{I=A,\,B,\,C,\,\ldots}^{N_c} v_{kI}^{i\,i}\,I \qquad (17)$$

where, v_{kI} is the stiochiometric coefficient for species component I in the elementary reaction k. The rate of production / consumption, S_I, for species component I can be computed as the sum of the rate of progress for all the elementary reactions in which component I participates:

$$S_I=M_{wI}\sum_{k=1}^{K}(v_{kI}^{ii}-v_{kI}^{i})\,\dot{w}_k \qquad (18)$$

Where, M_{wI} is molecular weight of species component I and $\dot{w}_k$ is the elementary reaction rate of progress for reaction, which can be calculated using combined combustion model.

The liquid kerosene fluid flow (dispersed phase fluid) is treated along with gaseous phase through Lagrangian Particle Tracking Method (LPTM). Eddy dissipation combustion model [19] is used for modeling turbulence-chemistry interaction in the scramjet combustor. The chemistry of the air and liquid hydrocarbon ($C_{12}H_{23}$) reaction is represented on a molar basis by,

$$C_{12}H_{23}+17.75\,(O_2+0.6H_2O+2.64N_2)\rightarrow 12CO_2+22.15H_2O+46.86N_2 \qquad (19)$$

The mixing rate determined from the EDM combustion model is given as

$$\dot{w}_{C_{12}H_{23},edm} = -A_{ebu}\,\bar{\rho}\,\frac{\varepsilon}{k}\,\min\left\{Y_f, \frac{Y_o}{v_s}, B_{ebu}\,\frac{Y_p}{1+v_s}\right\} \quad (20)$$

Where, Y_f, Y_o and Y_p are the mass fractions of fuel, oxidizer and products respectively, A_{ebu} and B_{ebu} are the model constants taken to be 4.0 and 0.5 respectively and v_s is the stoichiometric ratio. As the combustion in the scramjet combustor is mostly mixing limited, we used mixing controlled combustion model based on fast chemistry to model turbulence chemistry interaction. The model was tested extensively for number of high speed reacting cases for hydrogen and hydrocarbon fuels pertaining to scramjet flow [7-10, 20-25] and it was found that surface pressure and temperature is higher in the reaction zone because of instantaneous reaction on mixing. The surface pressure matches very well (within 5%) in the divergent portion of the combustor where the maximum thrust is produced. Since, the predicted temperature is higher in the reaction zone; the predicted thermal characteristics will be conservative. Although, the finer details of the combustion process (kinetic controlled phenomena like ignition, soot formation etc) could not be predicted in this approach, it is adequate to predict the performance and heat transfer characteristics of the combustor for engineering design.

Heat Flux Modelling Near the Wall

Launder and Spalding [26] wall-function approach is used for prediction of heat flux near wall in the present work. This approach connects the wall conditions (e.g., the wall-shear-stress) to the dependent variables at the near-wall mesh node which is presumed to lie in the fully-turbulent region of the boundary layer.

The logarithmic relation for the near wall velocity is given by:

$$u^+ = \frac{U_y}{u_\tau} = \frac{1}{\kappa}\ln(y^+) + C$$

where

$$y^+ = \frac{\rho\,\Delta n\,u_\tau}{\mu} \text{ and } u_\tau = \left(\frac{\tau_\omega}{\rho}\right)^{\frac{1}{2}} \quad (21)$$

u^+ is the near wall velocity, u_τ is the friction velocity, ρ is density, U_t is the known tangent velocity to the wall at a distance of Δn from the wall, y^+ is the dimensionless distance from the wall, κ is the von Karman constant and C is a log-layer constant depending on wall roughness.

The wall heat flux is modelled using thermal law-of-the-wall function approach of Kader [27]. The heat flux distribution (q_w) near-wall is calculated as:

$$q_w = \frac{\rho\,C_p\,u_\tau}{T^+}\,(T_w - T_f) \quad (22)$$

where,

$$T^+ = \frac{T}{T_w} = Pr\times y^+ \times e^{(-\Gamma)} + [\,2.12\times ln(y^+) + \beta\,]\times e^{(-\Gamma)}$$

$$\beta = (3.85\,pr^{1/3} - 1.3)^2 + 2.12\times ln(Pr),$$

$$Pr = \frac{\mu\,C_p}{\lambda},\ u_\tau = \left(\frac{\tau_w}{\rho}\right)^{1/2}$$

$$\Gamma = \frac{0.01\times(Pr\times y^+)^4}{1+5\times Pr^5\times y^+} \text{ and } y^+ = \frac{\rho\,\Delta n\,u_t}{\mu}$$

Validation Case : Convergent-Divergent (CD) Nozzle

Back et al. [17] conducted experiments over a wide range of stagnation pressures (2 - 30 bar) and stagnation temperatures (600 - 1200 K) to investigate the convective heat transfer in a water cooled convergent-divergent nozzle. Compressed heated air is passed through a long chamber into the nozzle. Thirty two pressure probes and twenty one thermocouple plugs were employed to measure static pressure, wall temperature and heat fluxes along the nozzle surface. Uncertainty and repeatability of these measurements were reported to be 5% and 2% respectively. Throat diameter of the nozzle is 0.0458 m with contraction ratio of 7.75 to 1.0 and expansion ratio of 2.68 to 1.0. The same geometry is taken as the validation test case for the present work and is shown in Fig.1.

A 90° sector is considered for the computation. Multi-block structured grids (0.83 million hexahedral cell) are made using ICEM-CFD software [28]. The grids are fine near the nozzle wall (average y^+ ~ 2) while relatively coarse grids are provided in the remaining portion of the nozzle. Consistent to experimental condition, stagnation pressure of 10.38 bar and stagnation temperature of 824 K are imposed at the nozzle entry. Isothermal wall (T_w = 467K) and supersonic outflow boundary conditions are

specified at nozzle walls and at nozzle exit respectively. Log-normalized maximum residue of 10^{-4} and global mass, momentum, and energy imbalance less than 0.1% between outlet and inlet planes are considered as the convergence criteria.

The different grids; namely, 0.55 million (coarse grid) and 0.83 million (fine grid) are used to carry out grid sensitivity study. Although the total number of points in the fine grid are less than a factor of 2 compared to coarse grid, the grid enrichment is mostly done near the nozzle wall. Minimum y^+ for fine and coarse grids is 1 and 3 respectively. The computed heat fluxes for two grids are compared along with experimental results in Fig.2. A good comparison between computation and experiment is obtained. The good match of convective heat flux for both the grids demonstrates the grid independence of the results.

Application : A Practical Scramjet Combustor

A demonstration mission for autonomous functioning of scramjet powered cruise hypersonic air-breathing vehicle flight for 20 seconds duration at Mach 6.5 and altitude 32 km is explained in Ref. [29]. Liquid hydrocarbon fuel is injected through row of struts placed in the combustor flow path. The development and testing of the scramjet combustor were restricted to half scale module due to limitation of the connected pipe mode test facility. High enthalpy airflow with total temperature of 1650-1750 K and total enthalpy of 1.55-1.65 MJ/kg from a vitiated air heater (hydrogen burner with oxygen replenishment) was accelerated through a contoured convergent-divergent nozzle to reach Mach ~2.0 at combustor entry.

Total length of the combustor including facility nozzle is 26 h (h is the combustor entry height). The schematic of the scramjet combustor is shown in Fig.3. The length of the initial constant area section (Section I) is h. The subsequent sections (Section II, III and IV) are having lengths 2.3h, 8.1h and 10h and top wall divergence 1°, 4° and 7.5° respectively.

In the simulation, X-axis is taken along the flow direction (length of combustor), while, Y and Z-axes are chosen along the height and width of the combustor respectively, with the origin being placed at the intersect point between left and bottom wall at combustor entry (Fig.3a). Liquid hydrocarbon ($C_{12}H_{23}$) is injected through number of 0.5 mm injection holes provided in the struts. The struts are arranged in such a manner that total amount of fuel is not injected at a particular axial location to avoid thermal choking. Table-1 provides the inflow boundary conditions at facility nozzle and fuel. Liquid kerosene fuel is injected transversely into the combustor at an equivalence ratio (ϕ) of 0.9 with a Rosin-Rammler (RR) particle distribution of diameter D = 38.8 μm, dispersion spread parameter of 1.5 which is equivalent to 14.34 μm Sauter mean diameter (SMD) [30]. Liquid kerosene fuel properties are provided in Table-2. All walls are specified as isothermal/adiabatic conditions including struts and facility nozzle. Supersonic outflow boundary condition is applied at the exit of the combustor.

Multi-block structured grids (hexahedral) are made using ICEM-CFD software [28]. Very fine grids are employed near the strut leading and trailing edges and com-

Table-1 : Inflow Boundary Conditions at Facility Nozzle and Fuel

Parameter	Facility Nozzle Entry	Fuel Injector Entry
Fluid	Vitiated air	Liquid Kerosene
Stagnation temp., T_0 (K)	1734	300
Mach Number	0.15	0.2
Equivalence ratio, ϕ	---	0.9
Total No. of injections	---	104
O_2	0.24	0.0
H_2O	0.18	0.0
N_2	0.58	0.0
$C_{12}H_{23}$	0.0	1.0

Table-2 : Liquid Kerosene Fuel Property

Parameter	Value
Dynamic viscosity, μ (Pa s)	0.0015
Thermal conductivity, λ (W/m K)	0.14
Molecular weight (kg/kmol)	167
Density, ρ (kg/m^3)	780
Surface tension, σ (N/m)	0.028
Kinematic viscosity (m^2/sec)	1.923 x 10^{-6}

bustor wall regions, while grids are relatively coarser in the remaining portion of the domain.

Computation of heat flux requires the resolution of thermal boundary layer. Grid independence study is carried out by considering different grid sizes from 2.04 million (380 x 53 x 102) to 3.12 million (421 x 73 x 102) cells. The 1st grid point adjacent to wall Δn of is varied from 5 μm to 80 μm. Clustering of grid is done in all the four walls. For Δn of 5 μm, y^+ value is less than 1. The typical grid structure of the domain is also shown in Fig.3. Comparison of non-dimensional convective heat flux ($q_{w_{\max}}$ where, $q_{w_{\max}}$ is maximum heat flux at 1st strut leading edge) and top wall surface pressure ($P_w/P_{0_{CI}}$ where, $P_{0_{CI}}$ is the total pressure at combustor entry) along the flow direction near the mid plane (Z/h = 1.6) for isothermal (T_w = 600 K) reactive flow simulations is shown in Figs.4(a) and 4(b) respectively for different grids. Computed pressures are seen to be invariant with grid size and computed heat fluxes vary very little for $\Delta n \leq$ 10 μm demonstrating the grid independence of the results.

Results and Discussion

Transverse injection of liquid kerosene fuel at an equivalence ratio (ϕ) of 0.9 is considered for reacting flow simulations.

Reacting Flow Field analysis at Tw = 600 K

Mach number and static temperature (T/T_0) distribution at different axial locations (i.e., X/h = -4.07, 0.0, 3.48, 6.98, 10.46, 13.95, 17.44 and 21.51) are shown in Figs.5 (a) and (b) respectively. Mach number is found to decrease while temperature increases adjacent to the strut regions due to mixing, combustion and heat release of the fuel. Subsonic zones behind the struts are clearly seen in Fig.5(a). Local static temperature is increased by 67% at combustion intense zone due to heat release, (Fig.5(b)). In combustor downstream, Mach number is increased, while temperature is reduced due to expansion of supersonic flow. The mass flow average Mach number, static pressure ratio, temperature ratio and total pressure loss (ΔP_0) at the entry and exit of the combustor are calculated and provided in Table-3. Here, total pressure loss for a particular axial station (ΔP_{0x}) is defined as the difference in total pressure in between the facility nozzle entry ($P_{0_{NI}}$) and the particular axial location (i.e. $\Delta P_{0x} = P_{0_{NI}} - P_{0x}$). Total pressure loss with respect to nozzle entry total pressure ($P_{0_{NI}}$) is found to be about 4.3% in the facility nozzle while in the combustor alone it is about 61.2%.

Table-3 : Average Propery Values at Combustor Entry and Exit

Parameter	M	$P_s/P_{0_{CI}}$	T_s/T_0	ΔP_0 (%)
Combustor entry	2.2	0.117	0.535	4.3
Combustor exit	1.79	0.071	1.182	65.5

Mass fraction of the species CO_2 and O_2 at various axial locations (X/h = -4.07, 0.0, 3.48, 6.98, 10.46, 13.95, 17.44 and 21.51) are shown in Figs.6a and 6b respectively. Reaction occurs mostly adjacent to the left wall (seen from the flow direction) region of combustor, as observed in Fig.6a. Considerable amount of O_2 is found to remain un-burnt (Fig.6b) adjacent to the side wall regions of the combustor due to unavailability of sufficient fuel in these regions. Fuel droplets are vaporized completely within the combustor and no liquid droplet is found at the exit of the combustor. The combustor performance is presented in terms of thrust and combustion efficiency. Total thrust availed by the combustor is calculated from the difference in momentum between outlet to inlet of the combustor (i.e. $\Delta F = \{\dot{m}_t u_e + p_e A_e\} - \{\dot{m}_{air} u_{CI} + p_{CI} A_{CI}\}$). Combustion efficiency is defined as the ratio of the burnt fuel to the total amount of liquid fuel injected from the struts (i.e., $\eta_c = \frac{\dot{m}_t \times y_{CO_2} \times 0.31628}{\dot{m}_{C_{12}} H_{23}}$). Where, $\dot{m}_t$ and $\dot{m}_{air}$ are total amount of reacting hot air flow rate at combustor exit and vitiated air flow rate at combustor entry respectively and u, p, A and y are axial velocity, static pressure, cross sectional area and mass fraction respectively. Subscripts t, e and CI are total, exit and combustor inlet respectively. Overall combustor performance in terms of thrust per fuel flow rate (ΔF_{th}) and combustion efficiency are 813.79 (N/kg/sec) and 84.7% respectively.

Computed axial pressure distributions at top wall mid section (Z/h=1.6) for different isothermal conditions and adiabatic condition are compared with experimental data in Fig.7. Static pressure increases due to the reaction of the fuel at fuel injection regions, then, decreases continuously due to the expansion of supersonic flow. Overall a good match is observed except at combustion intense region

(X/h = 6.0 - 10.0), where, CFD slightly underpredicted the experimental value. Surface pressures do not change significantly for different wall conditions.

Present simulation deals with convective heat flux only. As pointed out by Hoffmann et al. [31] convective heat flux contribute maximum (~85%) to the total heat flux in liquid rocket motors. In the present case of scramjet combustion chamber, since the flow field is convection dominated, convective heat flux will contribute even more (~90%) to the total heat flux (Convective heat flux is 1.6 MW/m^2 out of total heat flux 1.8 MW/m^2). Convective heat flux distributions at bottom, left, right and top walls are shown in Figs.8(a) to 8(d) respectively. Higher heat flux zones are observed behind the struts (Fig.8(a)) and towards the top and bottom left wall corners. Right wall is shown comparatively lower heat flux values than left wall. Top and bottom walls look almost similar distribution of heat flux except last divergent section. The unequal distribution of the heat flux in the wall is due to the reaction pattern which is caused due to combustor geometry asymmetry (constant area at the beginning and expansion section towards the exit), introduction of significant three dimensionality due to fuel injection struts and asymmetry of fuel injection. Axial distributions of wall heat flux at various generators for all the four walls are compared in Fig.9. High heat flux values are obtained adjacent to the intense reaction zone (in the middle of the combustor). Leading edge of the left wall experiences very high heat flux. Top, bottom and left side walls are showing almost similar values of heat flux, whereas, right side wall has shown comparatively less value as the right side wall has faced less combustion zone compared to the other walls. Computed heat fluxes are used for thermo-structural analysis of scramjet combustor. Table-4 shows the comparison of average convective heat flux ($q_w/q_{w_{max}}$) values on the four walls for nonreacting and reacting flow for T_w = 600 K condition. Average heat flux values for the reacting flow are more than double than that of nonreacting flow.

Table-4 : Average Convective Heat Flux Values ($q_w/q_{w_{max}}$) on Combustor Walls for Reacting and Nonreacting Flows

	Bottom	Top	Left	Right
Nonreacting Flow	0.01	0.089	0.073	0.075
Reacting Flow	0.213	0.217	0.213	0.156

Effect of Wall Temperature on Combustor Walls

During scramjet operation, combustor wall temperature increases and causes the reduction of convective heat flux and the combustor wall temperature is not known a priori. Reacting flow simulation with isothermal wall temperature of T_w = 900 K is carried out to determine the effect of wall temperature on heat transfer characteristics. Fig.10(a) shows the comparison of local heat flux distribution (at Z/h=1.6) for top wall for two isothermal wall. Local heat transfer coefficient ($h_c = q_w/(T_{aw}-T_w)$) distribution (T_{aw} and T_w are the adiabatic and isothermal wall temperatures respectively) along the axial length (Fig.10(b)) is shown to scale with the difference of the adiabatic wall temperature (T_{aw}) and the wall temperature (T_w). Hence, for getting the heat transfer characteristics of the scramjet combustor, it is not required to carry out computations with different wall temperature. One simulation for adiabatic condition and one isothermal condition are sufficient. Heat flux for any other wall temperatures, can be obtained from heat transfer coefficient. The constancy of heat transfer coefficients with different wall temperatures and requirement of one adiabatic and wall isothermal temperature in getting the heat flux values have been discussed in great detail with number of validation cases in Ref.[31]. Computed heat fluxes provide input for thermo structural design of the scramjet combustor.

Conclusions

Heat transfer characteristics of a flight worthy scramjet combustor with liquid hydrocarbon fuel are numerically explored. Three dimensional RANS equations alongwith *SST-k*ω turbulence model and species transport equations are solved using commercial CFD software. Infinitely fast rate kinetics and Lagrangian particle tracking method is used for combustion of fuel. Validation exercise for nonreacting flow in a convergent-divergent nozzle reveals a very good match of computed convective heat flux rate with experimental data. Grid independence of the scramjet combustor simulation is demonstrated with different grids and different spacing of first grid point. It is found that although the surface pressure distributions remain invariant with different grid spacing but minimum spacing of 10 micron adjacent to the wall is necessary for accurate prediction of wall heat flux. For flight sized scramjet combustor, simulation captures all the pertinent features of reacting flow in the combustor. Regions behind the fuel injection struts experience higher heat flux compared to other zones in the combustor. It is observed that although the heat flux varies with different wall temperature, heat transfer coefficient distribution remains almost invariant.

The computed heat flux provides important input for thermo-structural design of scramjet combustor.

Acknowledgement

Authors would like to acknowledge the support of HSTDV Project and DOLP Teams of Defence Research and Development Laboratory (DRDL), Hyderabad during the course of the work.

References

1. Feri, A., "Review of Problems in Application of Supersonic Combustion", Journal of Royal Aeronautical Society, 68 (645), 1964, pp.575-597.

2. Waltrup, P.J., "Liquid-fueled Supersonic Combustion Ramjet: A Research Perspective", Journal of Propulsion and Power, 3 (6), 1987, pp.515-524.

3. Curran, E.T., "Scramjet Engines: The First Forty Years", Journal of Propulsion and Power, 17 (6), 2001, pp.1138-1148.

4. Edwards, T., "Liquid Fuels and Propellants for Aerospace Propulsion: 1903-2003", Journal of Propulsion and Power, 19 (6), 2003, pp.1089-1107.

5. Bouchez, M., Dufour, E. and Montazel, X., "Hydrocarbon Fueled Scramjet for Hypersonic Vehicles", AIAA Paper, 1998, 1589.

6. Dufour, E. and Bouchez, M., "Computational Analysis of a Kerosene Fueled Scramjet", AIAA Paper, 2001, 1817.

7. Manna, P., Ramesh, R. and Chakraborty, D., "Liquid Fueled Strut Based Scramjet Combustor Design - A Computational Fluid Dynamics Approach", Journal of Propulsion and Power, 24 (2), 2008, pp.274-281.

8. Manna, P., Dharavath, M., Sinha, P.K. and Chakraborty, D., "Optimization of a Flight-worthy Scramjet Combustor Through CFD", Aerospace Science and Technology, No.27, 2013, pp.138-146.

9. Dharavath, M., Manna, P., Sinha P.K. and Chakraborty, D., "Numerical Analysis of a Kerosene Fuelled Scramjet Combustor",ASME Journal of Thermal Science and Engineering Applications, 8 (8), 2016, pp.1-7. doi:10.1115/1-4030699.

10. Dharavath, M., Manna, P. and Chakraborty, D., "Tip to Tail Simulation of a Hypersonic Airbreathing Cruise Vehicle", Journal of Propulsion and Power, 31 (5), 2015, pp.1370-1379.
DOI : 10.2514 / 1.B35686.

11. Dharavath, M., Manna P. and Chakraborty, D., "Prediction of Heat Flux in a Scramjet Combustor with Kerosene Fuel Through CFD", Paper No-CP-37, Proceedings of 17th AESI-CFD Symposium held at National Aerospace Laboratries (NAL), Bangalore, August 11-12, 2015, pp.168-177.

12. Song, K.D., Choi, S.H. and Scotti, S.J., "Transpiration Cooling Experiment for Scramjet Engine Combustion Chamber by High Heat Fluxes", Journal of Propulsion and Power, 22 (1), 2006, pp.96-102.

13. Li, L., Fan, X. and Wang, J., "Measurements of Wall Heat Flux and Temperature in a supersonic model Combustor", AIAA Paper, 2011, 5916.

14. Kennedy, P.J. and Donbar, M., "Heat Flux Measurement in a Scramjet Combustor Using Direct Write Technology", AIAA Paper, 2011, 2330.

15. Zhang, C., Qin, J., Yang, Q., Zhang, S., Chang, J. and Bao, W., "Indirect Measurement Method of Inner Wall Temperature of Scramjet with a State Observer", Acta Astronautica, 115, 2015, pp.330-337. DOI:10.1016/j.actaastro.2015.05.030.

16. ANSYS CFX, Release 11.0: Installation and Overview, July 2007.

17. Back, L.H., Massier, P.F. and Gier, H.L., "Convective Heat Transfer in a Convergent Divergent Nozzle", Technical Report 32-415, Jet Propulsion Laboratory, California Institute of Technology, Pasadena CA, 1965.

18. Menter, F.R., "Two-equation Eddy-viscosity Turbulence Models for Engineering Applications", AIAA Journal, 32 (8), 1994, pp.1598-1605.

19. Magnussen, B. F. and Hjertager, B. H., "On Mathematical Modeling of Turbulent Combustion with Special Emphasis on Soot Formation and Combustion", Sixteenth Symposium (International) on Combustion, The Combustion Institute, 1976, pp.719-725.

20. Chandra Murty, M.S.R. and Debasis Chakraborty., "Effect of Injection Angle in Mixing and Combustion Characteristics of Scramjet Combustor", International Journal of Hypersonics, Vol.2, No.1-2, 2011, pp.15-27.

21. Rahul Ingle and Debasis Chakraborty., "Numerical Simulation of Dual Mode Scramjet Combustor with Significant Upstream Interaction", International Journal of Manufacturing, Materials, and Mechanical Engineering, Vol.2, No.3, July-September 2012, pp.60-74.

22. Chandra Murty, M.S.R. and Debasis Chakraborty., "Numerical Simulation of Angular Injection of Hydrogen Fuel in Scramjet Combustor", Proc. I Meche, Part G, Journal of Aerospace Engineering, Vol. 226, No.7, July 2012, pp.861-872.

23. Malsur Dharavath., Manna, P. and Debasis Chakraborty., "Study of Mixing and Combustion in Scramjet Combustor with Ethylene Fuel Through CFD", Acta Astronautica, Vol.117, 2015, pp.305-318.

24. Ramesh Behera and Debasis Chakraborty., "Numerical Simulation of Kerosene Fueled Ramp Cavity Based Scramjet Combustor:", Journal of Aerospace Sciences and Technologies, Vol.58, No.2, May 2006, pp.104-111.

25. Manna, P., Ramesh Behera and Debasis Chakraborty., "Thermochemical Exploration of a Cavity Based Supersonic Combustor with Liquid Kerosene Fuel" Journal of Aerospace Sciences and Technologies, Vol.59, No.4, November 2007, pp.246-258.

26. Launder, B.E. and Spalding, D.B., "The Numerical Computation of Turbulent Flows", Comp Meth Appl Mech Eng, No.3, 1974, pp.269-289.

27. Kader, B.A., "Temperature and Concentration Profiles in Fully Turbulent Boundary Layers", International Journal of Heat and Mass Transfer, 24 (9), 1981, pp.1541-1544.

28. ICEM-CFD software, Release 11.0: Installation and Overview, January 7th, 2007.

29. Pannerselvam, S., Thiagarajan, V., Ganesh, A.T.K., Geetha, J.J., Ramanujachari, V. and Prahlada., "Airframe Integrated Scramjet Design and Performance Analysis", ISABE Paper, 2005, 1280.

30. Lefebvre, A.H., "Atomization and Sprays", Hemisphere Publishing Corporation, Bristol, First Edition, 1989.

31. Hoffmann, K.A., Siddiqui, M.S. and Chiang, S.T., "Difficulties Associated with the Heat Flux Computations of High Speed Flows by the Navier-stokes Equations", AIAA Paper, 1991, 0467.

32. Bhandarkar, A., Dharavath , M., Murty, M.S.R.C., Manna, P. and Chakraborty, D.., "A Novel CFD Method to Estimate Heat Transfer Coefficient for High Speed Flows", Defense Science Journal, 66 (3), 2016, pp.203-209. doi:10.14429/dsj/66.8873.

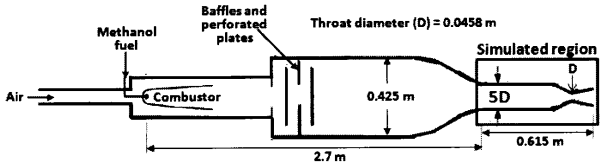

Fig.1 Experimental Setup with Simulated Region for CFD

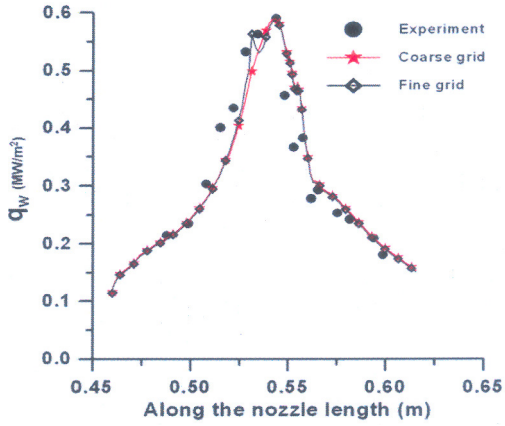

Fig.2 Comparison of Heat Flux with Test Data [17]

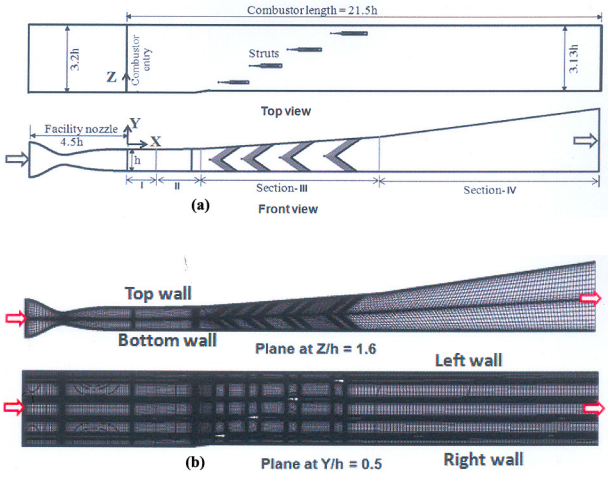

Fig.3 Schematic Diagram of Scramjet Combustor and Typical Grid Distribution

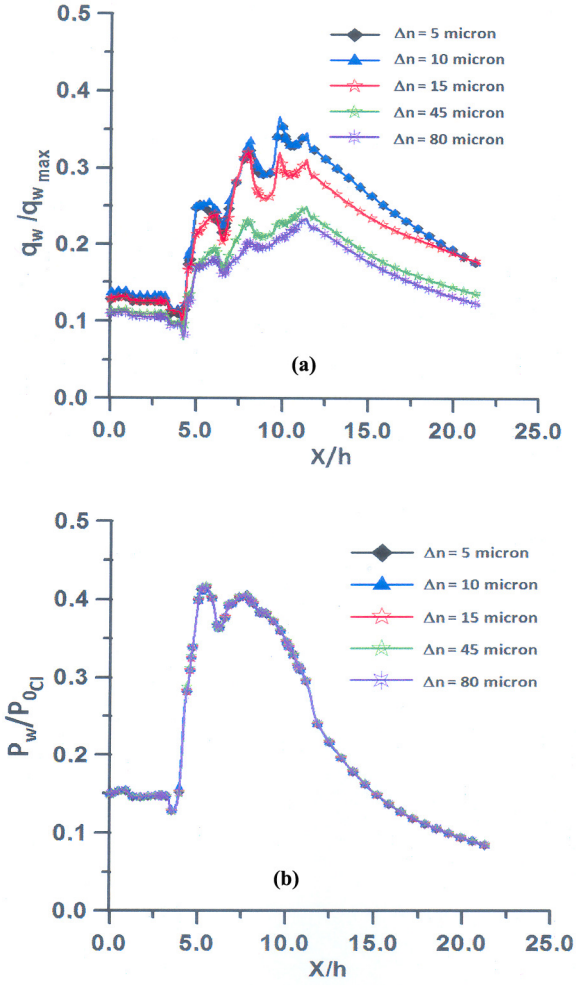

Fig.4 Comparison of Axial Distribution of (a) Heat Flux and (b) Top Wall Sjurface Pressures for Various Grid Sizes at Z/h = 1.6

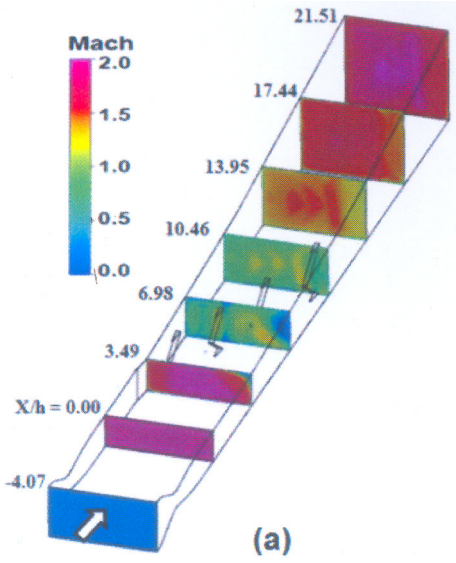

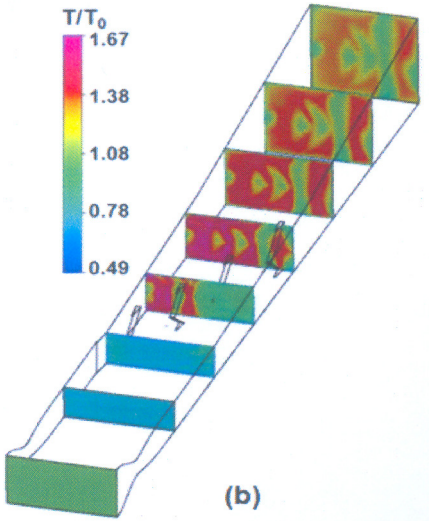

Fig.5 Distribution of (a) Mach Number (b) Static Temperature at Different Axial Locations

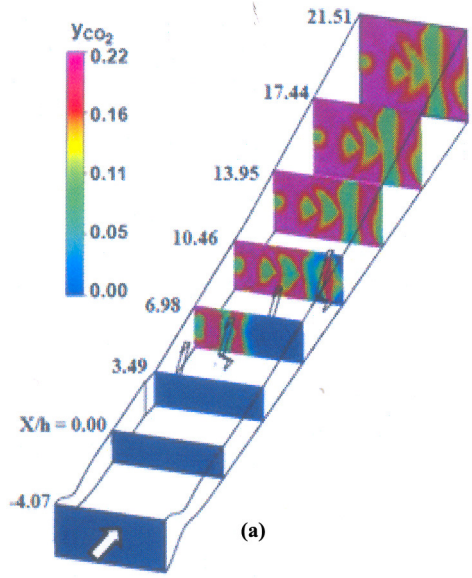

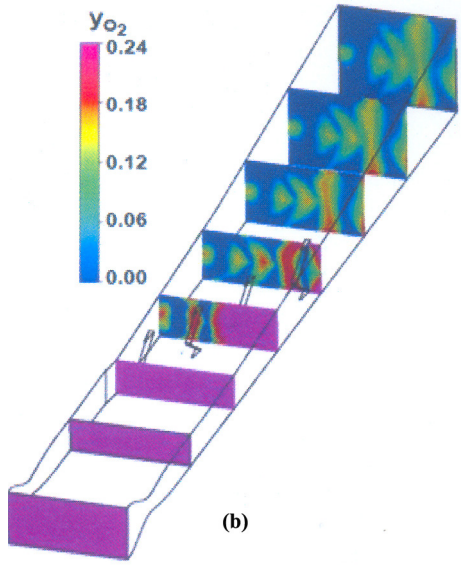

Fig.6 Various Species Mass Fraction Distributions at Different Axial Locations (a) CO_2 (b) O_2

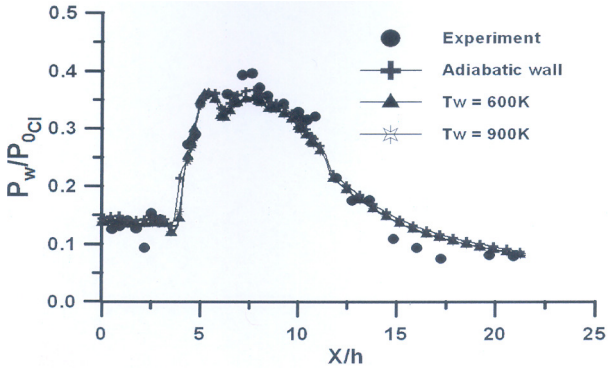

Fig.7 Comparison of Computed Top Wall Pressure Distribution at Mid Section (Z/h = 1.6) with Experiment

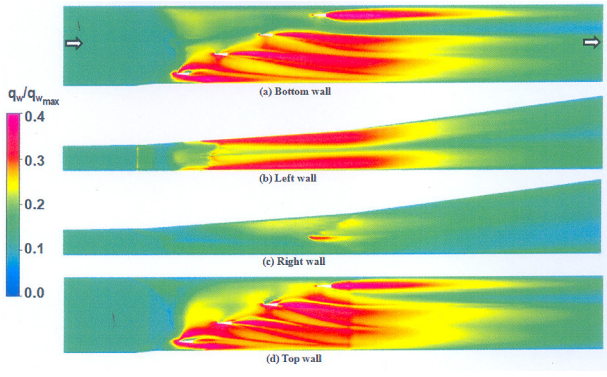

Fig.8 Contour of Heat Flux on Various Walls

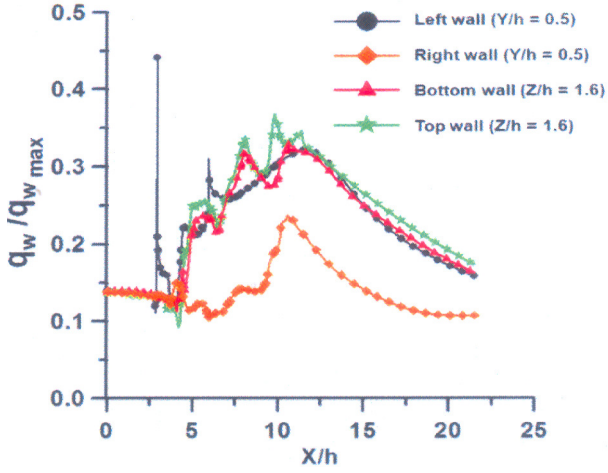

Fig.9 Heat Flux Distribution on Combustor Wall

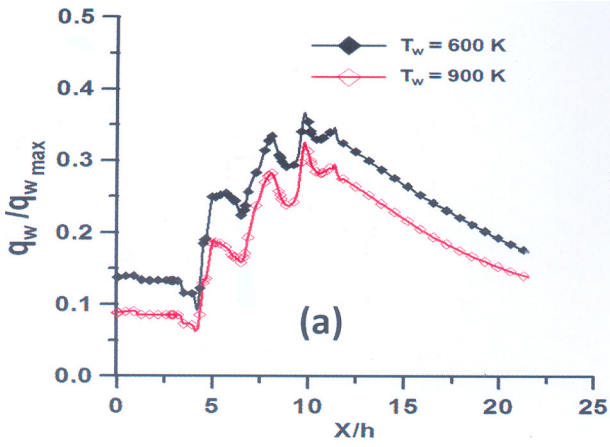

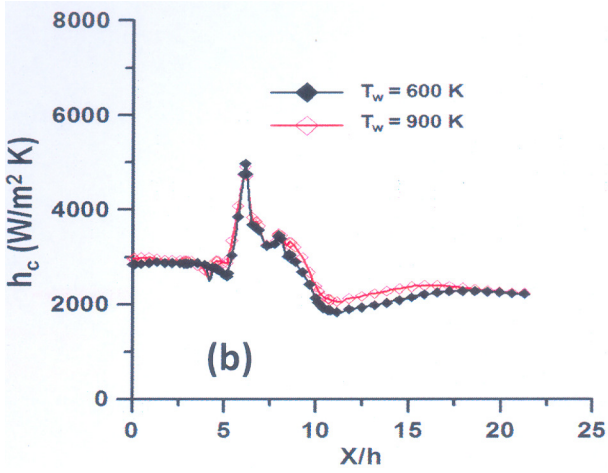

Fig.10 Comparison of Axial Distribution of (a) Heat Flux and (b) Heat Transfer Coefficient for Two Wall Temperatures